THE JOURNAL OF PHYSICAL CHEMISTRY B

Article

pubs.acs.org/JPCB

Macroscopic Modeling for Heat and Water Vapor Transfer in Dry Snow by Homogenization

Neige Calonne,*[,†,‡,§] Christian Geindreau,*[,‡,§] and Frédéric Flin[†]

[†]Météo-France − CNRS, CNRM-GAME UMR 3589, CEN, F-38400 Saint Martin d'Hères, France

[‡]3SR, Université Grenoble Alpes, F-38000 Grenoble, France

[§]3SR, CNRS, F-38000 Grenoble, France

Supporting Information

ABSTRACT: Dry snow metamorphism, involved in several topics related to cryospheric sciences, is mainly linked to heat and water vapor transfers through snow including sublimation and deposition at the ice−pore interface. In this paper, the macroscopic equivalent modeling of heat and water vapor transfers through a snow layer was derived from the physics at the pore scale using the homogenization of multiple scale expansions. The microscopic phenomena under consideration are heat conduction, vapor diffusion, sublimation, and deposition. The obtained macroscopic equivalent model is described by two coupled transient diffusion equations including a source term arising from phase change at the pore scale. By dimensional analysis, it was shown that the influence of such source terms on the overall transfers can generally not be neglected, except typically under small temperature gradients. The precision and the robustness of the proposed macroscopic modeling were illustrated through 2D numerical simulations. Finally, the effective vapor diffusion tensor arising in the macroscopic modeling was computed on 3D images of snow. The self-consistent formula offers a good estimate of the effective diffusion coefficient with respect to the snow density, within an average relative error of 10%. Our results confirm recent work that the effective vapor diffusion is not enhanced in snow.

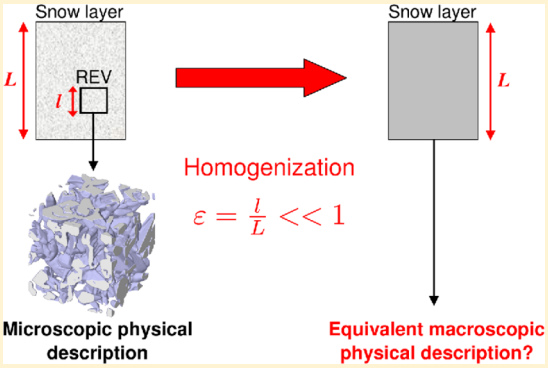

INTRODUCTION

The macroscopic modeling of heat and water vapor transfer through a snowpack is important to describe dry snow metamorphism and has important applications in snowpack stability,[1] transport of chemical species,[2] snow energy balance,[3] etc. Currently, the numerical resolution at the pore scale of the heat and water vapor transfer including phase change processes at the ice−pore interface is possible over small volumes only.[4−10] At the scale of a snow layer, a macroscopic equivalent model is more relevant.

In the literature, different macroscopic models have been proposed to describe such phenomena. Using a phenomenological approach, Albert and McGilvary[11] proposed to describe the heat and water vapor transfer through the snowpack by two coupled advection-diffusion equations including a source term due to the sublimation and deposition. Thanks to these equations, they investigated thermal effects due to air flow and vapor transport for different snow types and conditions. Following this work, Neumann et al.[12] performed several experiments in a cold room to determine the mass transfer coefficient that arises in the source term and plays an important role on the coupling between the temperature and the water vapor fields. In this way, they proposed an empirical expression of the mass transfer coefficient.

In parallel, several models[13−15] have been also developed to simulate the physical phenomena of the snowpack. As an example, in the Crocus model[16] the effective vapor diffusion is not described and the temperature is determined in dry snowpacks from a classical heat transfer equation without taking into account the latent heat due to phase change. The effective thermal conductivity is assumed constant within a snow layer and estimated with respect to density using the parametrization of Yen.[17] In the SNOWPACK model,[18] the effective vapor flux is simulated using an enhanced diffusion coefficient of snow (=8.5 × 10^{-5} m^2 s^{-1}, http://models.slf.ch).

As already mentioned, the above models have been established in a phenomenological way. Consequently, the link between these macroscopic modelings (e.g., effective properties or geometrical parameters involved) and the physical phenomena occurring at the pore scale is not always clearly established. As fully explained in Pinzer et al.,[19] the macroscopic description of the water vapor transfer in such models remains controversial. Studies by Yosida et al.,[20] Colbeck,[21] Sturm et al.,[22] and Satyawali et al.[23] indicate that the effective vapor diffusion in snow is greater than in a free air space, whereas Pinzer et al.[19] and Sokratov and Maeno[24] suggest a

Special Issue: Physics and Chemistry of Ice 2014

Received: May 28, 2014
Revised: July 10, 2014
Published: July 11, 2014

nonenhanced coefficient. In particular, from measurements and numerical simulations Pinzer et al.[19] indicate that the macroscopic vapor transfer through snow is not significantly influenced by the ice structure but mainly depends on the temperature field.

In this paper, we propose to derive the macroscopic equivalent modeling of the heat and vapor transfer through snow from its description at the pore scale (at the representative elementary volume (REV) scale) using the homogenization of multiple scale expansions.[25−29] Under the condition of separation of scales, the macroscopic equivalent modeling is obtained without any prerequisite at the macroscopic scale and is intrinsic to the geometry of the medium and the phenomenon. The method also provides the definitions of the effective parameters arising at macro scale and the domains of validity of the macroscopic modeling, given by the order of magnitude of the dimensionless numbers that characterize the intensity of the physical phenomena at the pore scale.

The paper is organized as follows: a step by step description of the homogenization method applied to the heat and water vapor transfer through snow is presented in the first section. The obtained macroscopic equivalent modeling is discussed. In a second section, the precision and robustness of the proposed macroscopic equivalent modeling is evaluated. For that purpose, a comparison of the numerical results for the heat and vapor transfer through a 2D snow layer obtained in the case of a fine scale modeling (i.e., by taking into account all the heterogeneities) and in the case of the corresponding macroscopic equivalent modeling is performed. Finally, the influence of the snow microstructure on the effective vapor diffusion tensor arising in the macroscopic modeling is investigated by performing numerical simulations on 3D images of different snow types.

DERIVATION OF THE MACROSCOPIC MODELING

Upscaling Method. Physical phenomena in heterogeneous media such as snow can be homogenized; i.e., they can be modeled by a continuous macroscopic equivalent description, if the condition of separation of scales is satisfied.[25−27,29] This fundamental condition may be expressed as

$$\varepsilon = \frac{l}{L} \ll 1 \tag{1}$$

where l and L are the characteristic lengths of the heterogeneities at the pore scale and of the macroscopic sample or excitation, respectively. This condition implies the existence of a REV of size l of both the material and the excitation. In the following, the macroscopic equivalent model is obtained from the description at the heterogeneity scale, i.e., the REV scale, by using the homogenization technique of multiple scale expansions[25,26] and by following the methodology presented in Auriault.[27] More precisely, the macroscopic equivalent modeling of heat and water vapor transfer through a snow layer is obtained from the description of the physics at the pore scale by (i) assuming the medium to be periodic, without loss of generality because the condition (1) is fulfilled;[30] (ii) writing the local description in a dimensionless form; (iii) evaluating the obtained dimensionless numbers with respect to the coefficient of separation of scale ε; (iv) looking for the unknown fields in the form of asymptotic expansions in powers of ε; (v) solving the successive boundary-value problems that are obtained after introducing these expansions in the local dimensionless description. The macroscopic equivalent model is obtained from compatibility conditions that are the necessary conditions for the existence of solutions to the boundary-value problems.

Description of the Physics at the Microscopic Scale. Let us assume that a snowpack can be represented by a collection of spatially periodic representative elementary volume with a characteristic length l, such that the scale parameter $\varepsilon = l/L \ll 1$ (Figure 1). Within the REV of snow Ω,

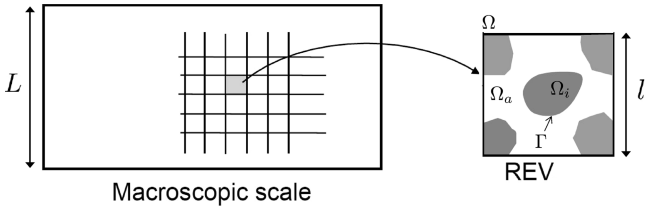

Figure 1. Macroscopic sample, i.e., a snow layer, and representative elementary volume (REV) with period Ω.

the domains occupied by the ice and the air are denoted by Ω_i and Ω_a respectively. The interface of ice is denoted by Γ and $\mathbf{n_i}$ is the unit outward vector of Ω_i. Neglecting the air convection and snow densification, the phenomena involved in dry snow metamorphism considered are (i) the heat conduction through ice and air, (ii) the water vapor diffusion in air, and (iii) the sublimation of ice and deposition of vapor at the ice−pore interface, which is characterized by the interface growth velocity.[9,31,32] In what follows, the subscripts "i" or "a" are related to quantities defined in Ω_i and Ω_a, respectively. Assuming that the properties of air and ice are isotropic, these physical phenomena at the pore scale are described by the following set of equations:

$$\rho_i C_i \frac{\partial T_i}{\partial t} - \operatorname{div}(\kappa_i \operatorname{grad} T_i) = 0 \text{ in } \Omega_i \tag{2}$$

$$\rho_a C_a \frac{\partial T_a}{\partial t} - \operatorname{div}(\kappa_a \operatorname{grad} T_a) = 0 \text{ in } \Omega_a \tag{3}$$

$$\frac{\partial \rho_v}{\partial t} - \operatorname{div}(D_v \operatorname{grad} \rho_v) = 0 \text{ in } \Omega_a \tag{4}$$

$$T_i = T_a \text{ on } \Gamma \tag{5}$$

$$\kappa_i \operatorname{grad} T_i \cdot \mathbf{n_i} - \kappa_a \operatorname{grad} T_a \cdot \mathbf{n_i} = L_{sg} \mathbf{w} \cdot \mathbf{n_i} \text{ on } \Gamma \tag{6}$$

$$D_v \operatorname{grad} \rho_v \cdot \mathbf{n_i} = (\rho_i - \rho_v) \mathbf{w} \cdot \mathbf{n_i} \simeq \rho_i \mathbf{w} \cdot \mathbf{n_i} \text{ on } \Gamma \tag{7}$$

where t is the time (s), T is the temperature (K), κ is the thermal conductivity (W m^{-1} K^{-1}), ρ is the density (kg m^{-3}), C is the specific heat capacity (J kg^{-1} K^{-1}), L_{sg} is the latent heat of sublimation (J m^{-3}), $\mathbf{w}$ is the interface growth velocity (m s^{-1}), ρ_v is the partial density of water vapor in air (kg m^{-3}), D_v is the water vapor diffusion coefficient in air (m^2 s^{-1}) and, div and grad are the divergence and gradient operators with respect to the physical space variable $\mathbf{X}$, respectively. At the interface, the heat and mass transfer are coupled through the normal interface growth velocity $w_n = \mathbf{w} \cdot \mathbf{n_i}$ (eq 6 and 7), which is given by the Hertz−Knudsen equation:

$$w_n = \mathbf{w} \cdot \mathbf{n_i} = \frac{1}{\beta}\left[\frac{\rho_v - \rho_{vs}(T_a)}{\rho_{vs}(T_a)} - d_0 K\right] \text{ on } \Gamma \tag{8}$$

dx.doi.org/10.1021/jp5052535 | J. Phys. Chem. B 2014, 118, 13393−13403

where β is the interface kinetic coefficient (s m^{-1}), ρ_{vs} is the saturation water vapor density in air (kg m^{-3}), d_0 is the capillary length (m), and K is the interface mean curvature (m^{-1}). Let us remark that the interface kinetic coefficient β is linked to the deposition coefficient α_d by $\beta = (1/\alpha_d)(\rho_i/\rho_{vs}(T_a))(2\pi m/kT_a)^{1/2}$, where m is the mass of a water molecule (kg) and k is the Boltzmann's constant equal to 1.38×10^{-23} J K^{-1}. Accurate experimental measurements of α_d, i.e. β, remain a challenge. In the literature,[9] β ranges from 10^4 to 10^9 s m^{-1}. On the basis of eq 8, w_n is positive when the ice surface grows and negative when the ice surface sublimates. The saturation vapor density ρ_{vs} is given by the Clausius–Clapeyron's law:

$$\rho_{vs}(T_a) = \rho_{vs}^{ref}(T^{ref}) \exp \frac{L_{sg} m}{\rho_i k}\left(\frac{1}{T^{ref}} - \frac{1}{T_a}\right) \quad (9)$$

The reference values T^{ref} and $\rho_{vs}^{ref}(T^{ref})$ are equal here to 273 K and 2.173×10^{-3} kg m^{-3}, respectively. In what follows, for the sake of simplicity, we will suppose that all material properties (ρ, C, κ, D_v, β, m) do not depend on the temperature.

Dimensionless Pore Scale Description: Normalization. Following the methodology presented in Auriault,[27] let us introduce into the set of eqs 2–7 the following representation of all dimensional variables φ: $\varphi = \varphi_c\varphi^*$, where the subscript "c" denotes characteristic quantities (constant) and the asterisk "*" denotes the dimensionless microscopic variables. So we have $\rho_i = \rho_{i_c}\rho^*$, $C_i = C_{i_c}C_i^*$, $\kappa_i = \kappa_{i_c}\kappa_i^*$, $T_i = T_{i_c}T_i^*$, $t = t_c t^*$, and so on. In the following, the microscopic length l is chosen as characteristic length ($l_c = l$); i.e., the so-called microscopic point of view is adopted.[27] The gradient and the divergence operator are thus replaced by $(1/l)$grad* and $(1/l)$div*. Consequently, the formal dimensionless set that describes the physics at the pore scale is written

$$[F_i^T]\rho_i^* C_i^* \frac{\partial T_i^*}{\partial t^*} - \text{div}^*(\kappa_i^* \text{ grad}^* T_i^*) = 0 \text{ in } \Omega_i \quad (10)$$

$$[F_a^T]\rho_a^* C_a^* \frac{\partial T_a^*}{\partial t^*} - \text{div}^*(\kappa_a^* \text{ grad}^* T_a^*) = 0 \text{ in } \Omega_a \quad (11)$$

$$[F_a^\rho]\frac{\partial \rho_v^*}{\partial t} - \text{div}^*(D_v^* \text{ grad}^* \rho_v^*) = 0 \text{ in } \Omega_a \quad (12)$$

$$T_i^* = T_a^* \text{ on } \Gamma \quad (13)$$

$$[K]\kappa_i^* \text{ grad}^* T_i^* \cdot \mathbf{n}_i - \kappa_a^* \text{ grad}^* T_a^* \cdot \mathbf{n_i} = [H] L_{sg}^* \mathbf{w}^* \cdot \mathbf{n}_i \text{ on } \Gamma \quad (14)$$

$$D_v^* \text{ grad}^* \rho_v^* \cdot \mathbf{n}_i = [W]\rho_i^* \mathbf{w}^* \cdot \mathbf{n}_i \text{ on } \Gamma \quad (15)$$

This dimensionless pore scale description introduces six dimensionless numbers that characterize the intensity of the physical phenomena at the pore scale. These dimensionless numbers are defined as

$$[F_i^T] = \frac{l^2 \rho_{i_c} C_{i_c}}{t_c \kappa_{i_c}} \qquad [F_a^T] = \frac{l^2 \rho_{a_c} C_{a_c}}{t_c \kappa_{a_c}} \qquad [F_a^\rho] = \frac{l^2}{D_{v_c} t_c} \quad (16)$$

$$[K] = \frac{\kappa_{i_c}}{\kappa_{a_c}} \qquad [H] = \frac{l L_{sg_c} w_{n_c}}{\kappa_{a_c} T_{a_c}} \qquad [W] = \frac{l \rho_{i_c} w_{n_c}}{D_{v_c} \rho_{v_c}} \quad (17)$$

Dimensionless numbers $[F_i^T]$ and $[F_a^T]$ correspond to the inverse of the Fourier number in Ω_i and Ω_a, respectively. These numbers characterize the ratio between the rate of thermal energy storage and the heat conduction rate. $[F_a^\rho]$ is an analogous inverse Fourier number for the transient water vapor transfer by diffusion in Ω_a. Dimensionless numbers [K], [H], and [W] are defined on the ice–pore interface. In particular, [H] characterizes the ratio between the heat flux induced by phase changes and the heat flux from heat conduction in the air phase. Similarly, [W] is defined as the ratio between the vapor flux from phase changes and the vapor flux from vapor diffusion in pores.

Estimation of the Dimensionless Numbers. The next important step of the homogenization process consists of estimating the above six dimensionless numbers with respect to the scale parameter $\varepsilon = l/L$. In practice, l and L correspond typically to the order of magnitude of the ice grain size and the thickness of a snow layer, respectively. In what follows, we assumed that $l \approx 5 \times 10^{-4}$ m and $L \approx 0.1$ m, leading to $\varepsilon = 5 \times 10^{-3}$. The characteristic values of each variable arising in the dimensionless numbers (16) and (17) are summarized in Table 1. These values were evaluated for a temperature of −10 °C and come from the literature.[9,33] According to these characteristic values, it can be first shown that the thermal diffusivity in the ice phase $\alpha_{i_c} = \kappa_{i_c}/(C_{i_c}\rho_{i_c})$ and in the air phase $\alpha_{a_c} = \kappa_{a_c}/(C_{a_c}\rho_{a_c})$, are of the same order of magnitude than the vapor diffusion coefficient D_{v_c}. Thus, the characteristic time t_c associated with these transfers through the snowpack are of the same order of magnitude: $t_c = O(L^2/\alpha_{i_c}) = O(L^2/\alpha_{i_a}) = O(L^2/D_{v_c})$. Consequently, from (16), we get

$$[F_i^T] = O([F_a^T]) = O([F_a^\rho]) = O(\varepsilon^2) \quad (18)$$

At the ice–pore interface, from (17), we have $[K] = O(1)$. Dimensionless numbers [H] and [W] depend on the intensity of the interface normal growth velocity w_{n_c}, which corresponds to an averaged value $\langle w_n \rangle$ over the REV. In practice, w_n varies widely locally inside a REV, depending on the temperature gradient, temperature, kinetic and curvature effects, etc. Nevertheless, several experimental and numerical studies[8,22,34–36] showed that w_n ranges from 0 to 10^{-9} m s^{-1} for

Table 1. Characteristic Values of the Properties Evaluated at −10 °C from the Literature[9,33]

symbol	description	value
T_{i_c}, T_{a_c}	temperature of ice, air	263 K
κ_{i_c}	heat conductivity of ice	2.3 W m^{-1} K^{-1}
κ_{a_c}	heat conductivity of air	0.024 W m^{-1} K^{-1}
C_{i_c}	specific heat capacity of ice	2000 J kg^{-1} K^{-1}
C_{a_c}	specific heat capacity of air	1005 J kg^{-1} K^{-1}
L_{sg_c}	latent heat of sublimation of ice	2.60×10^9 J m^{-3}
v_{n_c}	normal interface velocity	10^{-14} to 10^{-8} m s^{-1}
D_{v_c}	water vapor diffusion coefficient in air	2.036×10^{-5} m^2 s^{-1}
ρ_{v_c}	water vapor density in air	0.002 kg m^{-3}
ρ_{i_c}	ice density	917 kg m^{-3}
ρ_{a_c}	air density	1.335 kg m^{-3}
l	microscopic length	5×10^{-4} m
L	macroscopic length	0.1 m

dx.doi.org/10.1021/jp5052535 | J. Phys. Chem. B 2014, 118, 13393–13403

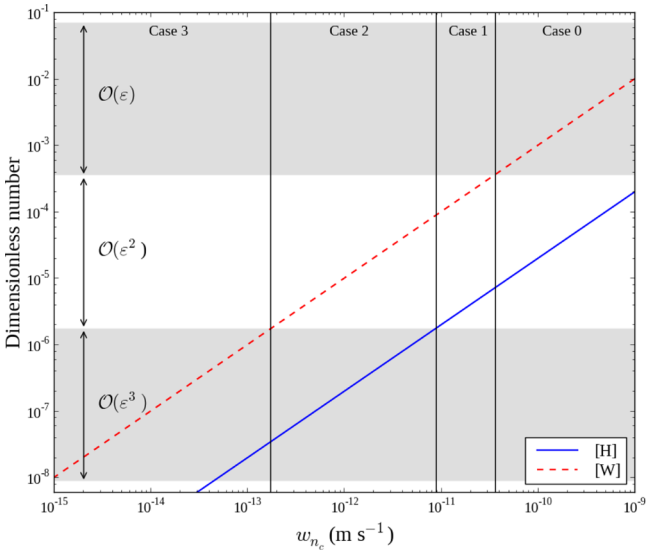

Figure 2. Estimation of dimensionless numbers [H] and [W] versus the characteristic interface normal growth velocity w_{n_c} from characteristic values given in Table 1.

temperature gradients between 0 and 500 K m^{-1}. Taking into account these results, Figure 2 shows that [H] and [W] can take different order of magnitude according to the value of w_{n_c}. Typically, several cases can be considered:

- Case 0: when $w_{n_c} \approx 10^{-10}$ m s^{-1}, [H] = $O(\varepsilon^2)$ and [W] = $O(\varepsilon)$
- Case 1: when $w_{n_c} \approx 10^{-11}$ m s^{-1}, [H] = $O(\varepsilon^2)$ and [W] = $O(\varepsilon^2)$
- Case 2: when $w_{n_c} \approx 10^{-12}$ m s^{-1}, [H] = $O(\varepsilon^3)$ and [W] = $O(\varepsilon^2)$
- Case 3: when $w_{n_c} \lesssim 10^{-13}$ m s^{-1}, [H] $\leqslant O(\varepsilon^3)$ and [W] $\leqslant O(\varepsilon^3)$

In what follows, we will not investigate the Case 0, which corresponds to the case of very large temperature gradients and is characterized by interfaces rapidly moving into vapor fields and significant latent heat effects. Only Cases 1, 2, and 3 are considered. Moreover, we will show that Cases 2 and 3 can be easily deduced from Case 1.

Asymptotic Analysis. The next step is to introduce multiple-scale coordinates.[25−27] The two characteristic lengths L and l introduce two dimensionless space variables, $\mathbf{x}^* = \mathbf{X}/L$ and $\mathbf{y}^* = \mathbf{X}/l$, where $\mathbf{X}$ is the physical space variable. The macroscopic (or slow) dimensionless space variable $\mathbf{x}^*$ is related to the microscopic (or fast) dimensionless space variable $\mathbf{y}^*$ by $\mathbf{x}^* = \varepsilon\mathbf{y}^*$. When l is used as the characteristic length, the dimensionless derivative operator grad* becomes $(\text{grad}_{y^*} + \varepsilon\ \text{grad}_{x^*})$, where the subscripts x^* and y^* denote the derivatives with respect to the variables $\mathbf{x}^*$ and $\mathbf{y}^*$, respectively. Following the multiple-scale expansion technique,[25−27] the ice temperature T_i^*, the air temperature T_a^*, and the water vapor ρ_v^* are sought in the form of asymptotic expansions of powers of ε:

$$\varphi^*(\mathbf{x}^*,\mathbf{y}^*,t) = \varphi^{*(0)}(\mathbf{x}^*,\mathbf{y}^*,t) + \varepsilon\varphi^{*(1)}(\mathbf{x}^*,\mathbf{y}^*,t) + \varepsilon^2\varphi^{*(2)}(\mathbf{x}^*,\mathbf{y}^*,t) + \ldots \quad (19)$$

where $\varphi^* = T_i^*$, T_a^*, ρ_v^* and the corresponding $\varphi^{*(i)}$ are periodic functions of period Ω with respect to the space variable $\mathbf{y}^*$. Substituting these expansions in the set (10)−(15) gives, by identification of like powers of ε, successive boundary value problems to be investigated. All the details concerning this asymptotic analysis of the Case 1 are presented in the Appendix A of the Supporting Information. The main results are summarized in the following section.

Macroscopic Equivalent Description. According to the order of magnitude of the dimensionless numbers in the Case 1, $[\mathrm{F}_i^T] = O([\mathrm{F}_a^T]) = O([\mathrm{F}_a^\rho]) = O(\varepsilon^2)$, [K] = $O(1)$, [H] = $O(\varepsilon^2)$, [W] = $O(\varepsilon^2)$, the asymptotic analysis presented in Appendix A of the Supporting Information shows that the heat transfer and the water vapor diffusion at the macroscopic scale are described by the eqs A.48 and A.51. Retuning in dimensional variables, the macroscopic model is written

$$(\rho C)^{\text{eff}}\frac{\partial T^{(0)}}{\partial t} - \text{div}(\mathbf{k}^{\text{eff}}\ \text{grad}\ T^{(0)}) = \text{SSA}_V L_{sg} w_n^{(0)} \quad (20)$$

$$\phi\frac{\partial \rho_v^{(0)}}{\partial t} - \text{div}(\mathbf{D}^{\text{eff}}\ \text{grad}\ \rho_v^{(0)}) = -\text{SSA}_V \rho_i w_n^{(0)} \quad (21)$$

where $w_n^{(0)}$ is given by the Hertz−Knudsen equation (A.47) and the Clausius−Clapeyron's law (A.43)

$$w_n^{(0)} = \frac{1}{\beta}\left[\frac{\rho_v^{(0)} - \rho_{vs}^{(0)}(T^{(0)})}{\rho_{vs}^{(0)}(T^{(0)})} - d_0 K\right] \quad (22)$$

$$\rho_{vs}^{(0)}(T^{(0)}) = \rho_{vs}^{\text{ref}}\ \exp\left[\frac{L_{sg} m}{\rho_i k}\left(\frac{1}{T^{\text{ref}}} - \frac{1}{T^{(0)}}\right)\right] \quad (23)$$

and where ϕ is the porosity, $\text{SSA}_V = |\Gamma|/|\Omega|$ is the specific surface area defined as the ice surface area over the snow volume in m^{-1}, $(\rho C)^{\text{eff}}$ is the effective thermal capacity (A.49), $\mathbf{k}^{\text{eff}}$ is the effective thermal conductivity tensor (A.50), and $\mathbf{D}^{\text{eff}}$ is the effective diffusion tensor (A.52). These effective properties are defined as

$$(\rho C)^{\text{eff}} = (1-\phi)\rho_i C_i + \phi\rho_a C_a \quad (24)$$

$$\mathbf{k}^{\text{eff}} = \frac{1}{|\Omega|}\left(\int_{\Omega_a} \kappa_a(\text{grad}\ \mathbf{t}_a + \mathbf{I})\ \mathrm{d}\Omega + \int_{\Omega_i} \kappa_i(\text{grad}\ \mathbf{t}_i + \mathbf{I})\ \mathrm{d}\Omega\right) \quad (25)$$

$$\mathbf{D}^{\text{eff}} = \frac{1}{|\Omega|}\int_{\Omega_a} D_v(\text{grad}\ \mathbf{g}_v + \mathbf{I})\ \mathrm{d}\Omega \quad (26)$$

where $\mathbf{t}_a$ and $\mathbf{t}_i$ are two periodic vectors solution of the following boundary value problem over the REV (A.20)−(A.24):

$$\text{div}(\kappa_i(\text{grad}\ \mathbf{t}_i + \mathbf{I})) = 0 \text{ in } \Omega_i \quad (27)$$

$$\text{div}(\kappa_a(\text{grad}\ \mathbf{t}_a + \mathbf{I})) = 0 \text{ in } \Omega_a \quad (28)$$

$$\mathbf{t}_i = \mathbf{t}_a \text{ on } \Gamma \quad (29)$$

$$(\kappa_i(\text{grad}\ \mathbf{t}_i + \mathbf{I}) - \kappa_a(\text{grad}\ \mathbf{t}_a + \mathbf{I}))\cdot\mathbf{n}_i = 0 \text{ on } \Gamma \quad (30)$$

$$\frac{1}{|\Omega|}\int_{\Omega}(\mathbf{t}_a + \mathbf{t}_i)\ \mathrm{d}\Omega = 0 \quad (31)$$

and where $\mathbf{g}_v$ is a periodic vector solution of the following boundary value problem over the REV (A.35)−(A.37):

$$\text{div}(D_v(\text{grad}\ \mathbf{g}_v + \mathbf{I})) = 0 \text{ in } \Omega_a \quad (32)$$

dx.doi.org/10.1021/jp5052535 | J. Phys. Chem. B 2014, 118, 13393−13403

$$D_v(\text{grad}\,\mathbf{g}_v + \mathbf{I})\cdot\mathbf{n}_i = 0 \text{ on } \Gamma \quad (33)$$

$$\frac{1}{|\Omega|}\int_{\Omega_a} \mathbf{g}_v \, d\Omega = 0 \quad (34)$$

In Case 1, the above macroscopic equivalent description shows that at the first order:

- the heat transfer through the snowpack is described by a transient heat transfer (eq 20) with a source term $Q_T = \text{SSA}_V L_{sg} w_n^{(0)}$ induced by the phase change process occurring at the pore scale on the ice−pore interface Γ.
- the mass transfer is governed by a transient water vapor diffusion (eq 21) including a source term $Q_V = -\text{SSA}_V \rho_i w_n^{(0)}$ induced by the phase change process occurring on Γ. Let us remark that $\rho_v^{(0)}$ is the vapor density per unit volume of fluid.
- both source terms are defined by the Hertz−Knudsen equation (eq 22) and the Clausius−Clapeyron's law (eq 23) but expressed with respect to the two macroscopic variables $T^{(0)}$ and $\rho_v^{(0)}$.

Finally, from the asymptotic analysis presented in the Appendix A of the Supporting Information, it can be easily shown that in Case 2, i.e., when $[H] = O(\varepsilon^3)$ and $[W] = O(\varepsilon^2)$, the macroscopic modeling is the same as the one obtained in the Case 1, but Q_T is negligible. Similarly, in Case 3, i.e., when $[H] \leqslant O(\varepsilon^3)$ and $[W] \leqslant O(\varepsilon^3)$, both Q_T and Q_v become negligible at the macroscopic scale.

2D NUMERICAL EXAMPLE

Problem Definition. To evaluate the obtained macroscopic modeling, we propose in this section to compare the numerical results for the heat and water vapor transfer through a snow layer obtained in the case of a fine scale modeling (i.e., by taking into account all the heterogeneities) and in the case of the corresponding macroscopic equivalent modeling. For that purpose, finite element numerical simulations have been preformed on the same 2D vertical snow layer of 10 cm length and 0.5 cm width (Figure 3) using the code ComsolMultiphysics. At the top and the bottom of the snow layer, the temperatures T_{top} and T_{bottom} are imposed and, by this way, the vapor density, which is supposed to be equal to the saturation vapor density, $\rho_{vs}(T_{top})$ and $\rho_{vs}(T_{bottom})$ using eq 9. Symmetry conditions are imposed on the lateral sides of the snow layer. In what follows, curvature effects are neglected ($d_0 K = 0$), and the interface kinetic coefficient β is taken constant and equal to 5.5×10^5 s m^{-1}, as in the study of Kaempfer and Plapp.[9]

In the case of the fine scale modeling, the snow layer microstructure consists in 200 periodic cells of 0.5×0.5 mm^2; each periodic cell (REV) is composed of an ice grain of diameter 0.3 mm surrounded by air. Thus, the porosity is equal to 0.71, which corresponds to a snow density of 266 kg m^{-3}. In this case, the heat and the mass transfer within this layer are described by the set of eqs 2−9 where T_i, T_a, and ρ_v are the unknowns. This set of equations has been numerically solved using the material parameter values presented in Table 1.

In the case of the macroscopic equivalent modeling, the snow layer is seen as a continuous equivalent medium. The heat and the mass transfer are now described by the set of eqs 20−23 where $T^{(0)}$ and $\rho_v^{(0)}$ are the macroscopic unknowns. This macroscopic description requires us to compute some parameters or effective properties over the REV. The porosity

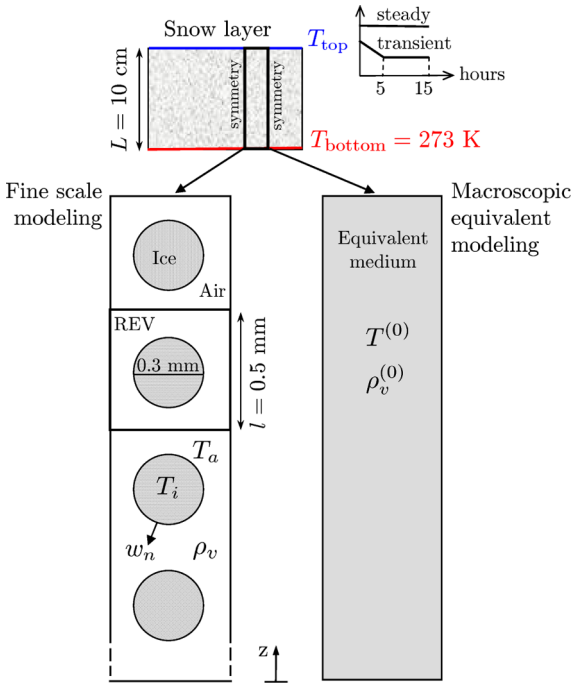

Figure 3. Illustration of the 2D geometry for the fine scale modeling and the macroscopic equivalent modeling.

ϕ and the specific surface area SSA_V involved in the macroscopic modeling can be easily deduced from the geometry of the REV. The effective heat capacity $(\rho C)^{eff}$, effective thermal conductivity $\mathbf{k}^{eff}$ and effective vapor diffusion $\mathbf{D}^{eff}$ were computed using relations 24−26, respectively. For that purpose, the boundary value problems (27)−(31) and (32)−(34) have been solved numerically over the REV. Due to the symmetry of the REV, tensors $\mathbf{D}^{eff}$ and $\mathbf{k}^{eff}$ are both isotropic and can be written $\mathbf{D}^{eff} = D^{eff}\mathbf{I}$ and $\mathbf{k}^{eff} = k^{eff}\mathbf{I}$, where $\mathbf{I}$ is the identity tensor. The parameters and the effective properties deduced from the REV scale are summarized in Table 2.

Table 2. Macroscopic Properties Computed over the REV of the Considered 2D Geometry, Using $\kappa_a = 0.024$ W m^{-1} K^{-1}, $\kappa_i = 2.3$ W m^{-1} K^{-1}, and $D_v = 2.036 \times 10^{-5}$ m^2 s^{-1}

porosity, ϕ	0.71
surface area, SSA_V	3770 m^{-1}
effective thermal capacity, $(\rho C)^{eff}$	5.328×10^5 J m^{-3} K^{-1}
effective thermal conductivity, k^{eff}	0.04243 W m^{-1} K^{-1}
effective diffusion, D^{eff}	1.156×10^{-5} m^2 s^{-1}

Results. Figure 4 shows the temperature field and vapor density field as well as the vapor density flux at the interface computed within the cell at midheight of the snow layer using the fine scale modeling when $T_{top} = 263$ K and $T_{bottom} = 273$ K, in the steady state. At the pore scale, the temperature gradient is mainly concentrated in air due to the ratio κ_i/κ_a, which is around 100. The vapor flux varies widely along the interface and the sign is opposite between the upper (sublimation) and lower (deposition) parts of the grain.

The vertical profiles of the temperature and vapor density through the snow layer obtained in the case of a fine scale modeling (marks) and in the case of the corresponding macroscopic equivalent modeling (solid line) are presented in

dx.doi.org/10.1021/jp5052535 | J. Phys. Chem. B 2014, 118, 13393−13403

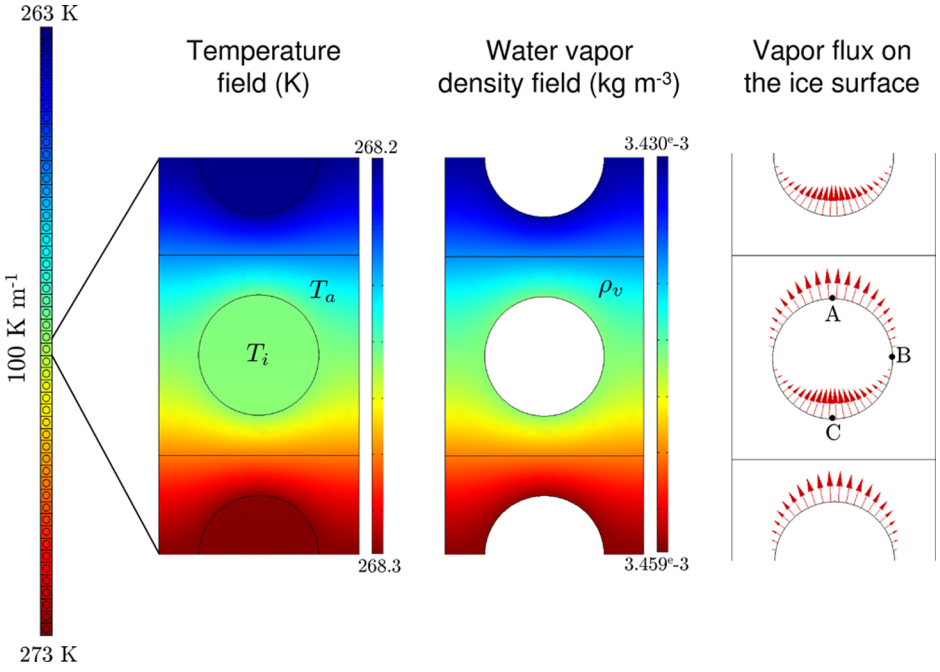

Figure 4. Microscopic field of temperature, water vapor density, and vapor density flux computed within the cell at midheight of the snow layer that experiences a constant temperature gradient of 100 K m^{-1}.

Figures 5 and 6. In the case of the fine scale modeling, the average values of each microscopic variable over the cell have been reported, expressed as

$$\langle T \rangle = \frac{1}{\Omega}\left(\int_{\Omega_i} T_i \, d\Omega + \int_{\Omega_a} T_a \, d\Omega\right)$$

$$\langle \rho_v \rangle = \frac{1}{\Omega_a}\int_{\Omega_a} \rho_v \, d\Omega$$

Figure 5 shows the obtained results in the steady state, when T_{bottom} = 273 K and T_{top} = 268, 263, and 248 K successively, which leads to a temperature gradient of 50, 100, and 250 K m^{-1}, respectively. Under such conditions, temperature profiles are mostly linear; by contrast, vapor density profiles are strongly nonlinear. Moreover, this figure shows that overall the temperature and water vapor profiles deduced from the fine scale modeling and the macroscopic equivalent modeling are close. In detail, the macroscopic equivalent description underestimates the temperature and vapor density; as shown in Figure 5, the maximum relative difference between both modelings does not exceed 0.24% for the temperature and 5.44% for the vapor density in the middle of the snow layer and for T_{top} = 248 K. This figure also underlines that a small error on the temperature field may lead to a large error on the water vapor field when the temperature gradient increases.

Figure 6 shows the temperature and vapor density profiles in the case of a transient analysis. The snow layer is initially at a temperature of 273 K; then T_{top} decreases to reach 263 K in 5 h and remains constant until 15 h. The value of T_{bottom} is constant and equal to 273 K. The profiles at six different times are shown. Once again, we can observe a good agreement between the numerical results of both modelings. Under such conditions, the maximum relative error is obtained at t = 6 h and reaches −0.14% for the temperature profile and −3.35% for the vapor density profile.

Finally, the temperature and water vapor profiles (dashed lines) obtained if the source term is supposed to be negligible in the macroscopic heat transfer equation (Case 2) are also reported in Figure 5. These results show that for low to moderate temperature gradients (typically lower than 100 K m^{-1}), the relative difference between both modelings remains lower than 0.1% for the temperature and lower than 2.2% for the water vapor density. For large temperature gradients (typically larger than 200 K m^{-1}), these relative differences strongly increase and show that the source term in the heat transfer equation is not negligible. These results are consistent with the dimensionless analysis and are directly linked to the evolution of the normal growth velocity with respect to the temperature gradient.

Figure 7 presents the evolution of the normal growth velocity at the midheight of the snow layer deduced from the fine scale modeling (w_n at the top (point A), base (point C), and midheight (point B) of the ice grain as well as the average value $\langle w_n \rangle$ over the REV, Figure 4) and from the macroscopic equivalent modeling ($w_n^{(0)}$) for a temperature gradient within the range 0 to 250 K m^{-1}. As expected, the normal growth velocity increases with increasing temperature gradient. At the top and the base of the ice grain, w_n is negative (sublimation) and positive (deposition), respectively, and ranges typically from 10^{-11} to 10^{-9} m s^{-1}, whereas at the midheight of the grain w_n ranges from 10^{-15} to 10^{-12} m s^{-1}. Figure 7 shows that the average value $\langle w_n \rangle$ over the REV presents a similar trend and also ranges from 10^{-15} to 6×10^{-12} m s^{-1}. The averaged growth velocity over the particle interface is low, but positive, meaning that the deposition predominates slightly over the sublimation. This is due to the nonlinear relationship between the temperature and the saturation vapor density. The evolution of the "macroscopic equivalent normal velocity" $w_n^{(0)}$ is consistent with $\langle w_n \rangle$. This evolution of the normal velocity versus the temperature gradient confirms that the dimensionless numbers [H] and [W] may extend over several orders of magnitude, as already discussed. For large temperature gradients, $[H] = O(\varepsilon^2)$ and $[W] = O(\varepsilon^2)$, which corresponds

dx.doi.org/10.1021/jp5052535 | J. Phys. Chem. B 2014, 118, 13393−13403

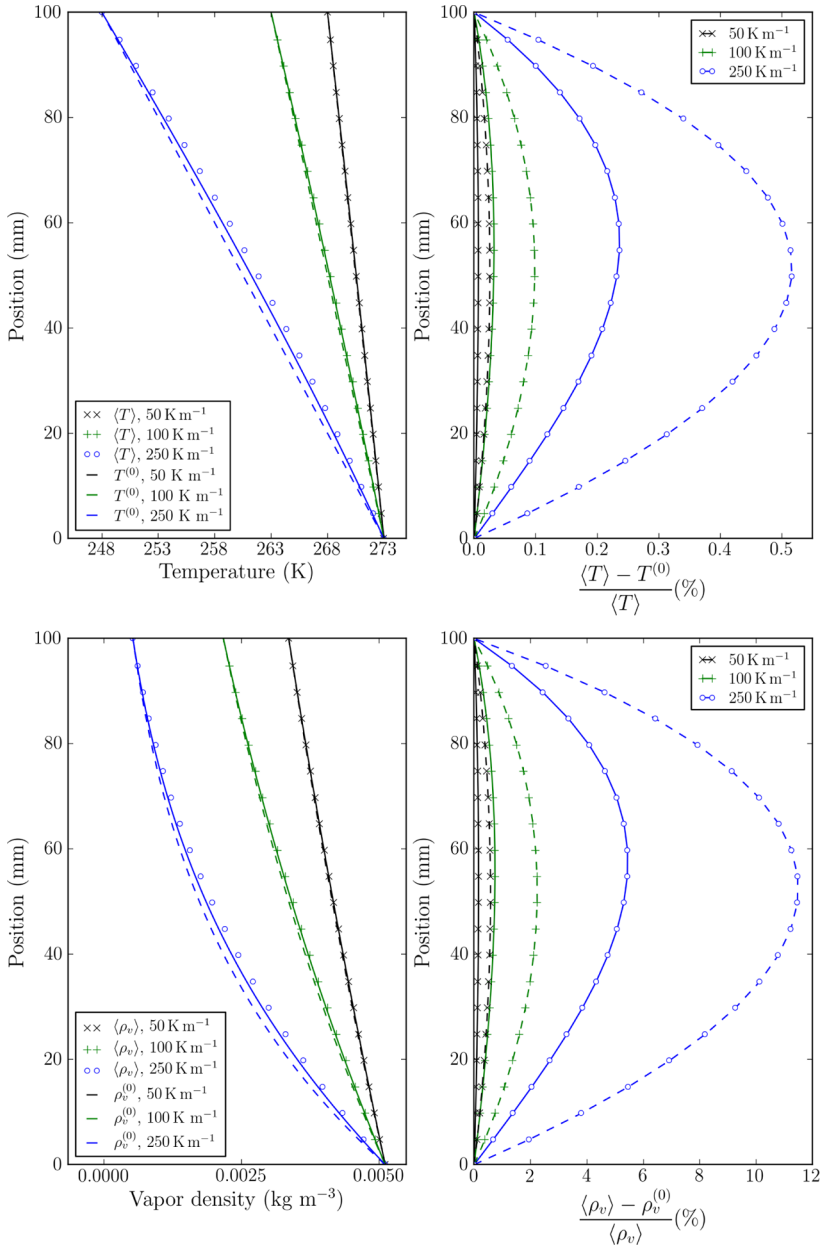

Figure 5. Comparison between fine scale (marks) and macroscopic equivalent (solid line) modeling (Case 1) in the steady state: vertical profile of temperature and vapor density and relative errors for a temperature gradient of 50, 100, and 250 K m^{-1}. Dashed lines correspond to Case 2: the source term is supposed to be negligible in the macroscopic heat transfer equation.

to Case 1, i.e., the macroscopic modeling including a source term in both the heat and mass transfer equation.

EFFECTIVE DIFFUSION TENSORS FROM 3D IMAGES OF SNOW

In practice, the macroscopic equivalent modeling given by the set of eqs 20−23 requires the knowledge of the effective thermal conductivity tensor $\mathbf{k}^{\text{eff}}$ and the effective vapor diffusion tensor $\mathbf{D}^{\text{eff}}$, which can be computed not only on a simple microstructure as previously but also on 3D images of snow obtained by X-ray microtomography. The effective thermal conductivity tensor has been already computed on 3D images in Calonne et al.[37] Following this work, the effective vapor diffusion tensor was computed by solving the specific boundary value problem 32−34 over REVs extracted from 3D images using the software Geodict (see www.geodict.de/DiffuDict.php). First, we estimated the size of the REVs following Calonne et al.[37] (auxiliary material) by computing the effective vapor diffusion tensor over subvolumes of increasing sizes. The effective vapor diffusion tensor has been determined on 35 images of snow spanning the different snow types and a large range of snow density (more information about the 3D images can be found in the auxiliary materials of Calonne et al.[38]). Three subvolumes of the 3D images used are shown in Figure 8. Each image has been defined in a frame (x, y, z), where z is the vertical direction of the snow layer. In the following, we only present the diagonal components of the tensor $\mathbf{D}^{\text{eff}}$, because the nondiagonal ones are negligible.

Figure 9 shows the evolution of the vertical and horizontal components of $\mathbf{D}^{\text{eff}}$ normalized by the vapor diffusion coefficient in the air (D_v) as a function of the snow density. These values are given in Appendix B of the Supporting

dx.doi.org/10.1021/jp5052535 | J. Phys. Chem. B 2014, 118, 13393−13403

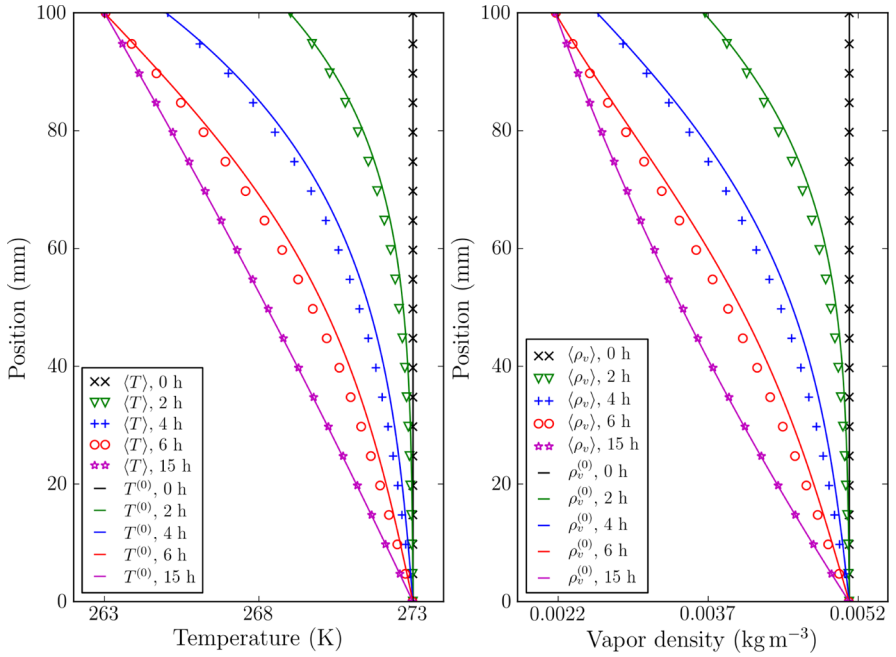

Figure 6. Comparison between fine scale (marks) and macroscopic equivalent (continuous lines) modeling in the case of transient analysis: vertical profile of temperature and water vapor density within the snow layer at six different times.

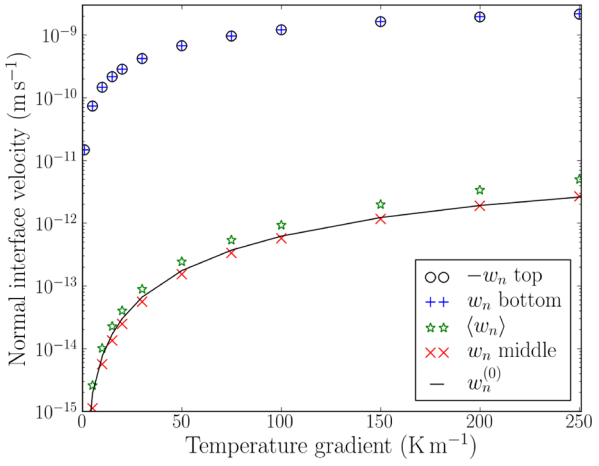

Figure 7. Evolution of the normal growth velocity in the midheight of the 2D snow layer deduced from the fine scale modeling (w_n at the top, base and middle of the ice grain as well as the average value $\langle w_n\rangle$ over the REV) and from the macroscopic equivalent modeling ($w_n^{(0)}$) for a temperature gradient within the range 0−250 K m^{-1}.

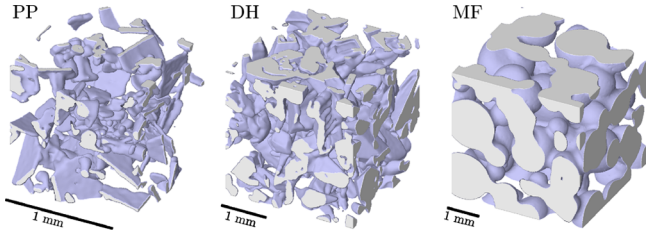

Figure 8. Representation of 3D images (subvolumes) of three different snow types obtained by X-ray tomography: precipitation particles (PP), depth hoar (DH), and melt forms (MF), from left to right.

Information. Horizontal components correspond to the average of the x-value and y-value of $\mathbf{D}^{\text{eff}}$. In the figure, the vertical and horizontal components are represented by the tips and

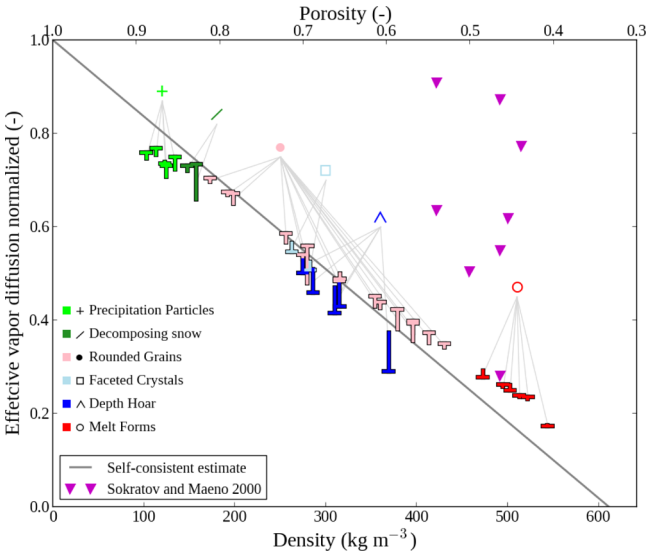

Figure 9. Normalized effective vapor diffusion versus snow density. Tips and horizontal bars of the "T" shapes represent the vertical and horizontal components of $\mathbf{D}^{\text{eff}}$. Colors correspond to the ICSSG.[39] Measurements from Sokratov and Maeno[24] are shown in purple, and the self-consistent estimate is plotted in gray.

horizontal bars of the "T" shapes, respectively. Let us remark that $\mathbf{D}^{\text{eff}}/D_v = \phi\tau_a$, where τ_a is the tortuosity tensor associated with the air phase and ϕ is the porosity. The normalized effective vapor diffusion decreases linearly with increasing density and ranges from 0.17 to 0.76, which correspond to non-normalized values from 3.46×10^{-6} to 1.55×10^{-5} m^2 s^{-1}, if we consider $D_v = 2.036 \times 10^{-5}$ m^2 s^{-1}.

We quantified the anisotropic behavior of the effective vapor diffusion of snow by using an anisotropy coefficient. This coefficient is defined as the vertical component over the horizontal component of the diagonal terms of the tensor $\mathbf{D}^{\text{eff}}$. Figure 10 shows the anisotropy coefficient of the effective vapor

dx.doi.org/10.1021/jp5052535 | J. Phys. Chem. B 2014, 118, 13393−13403

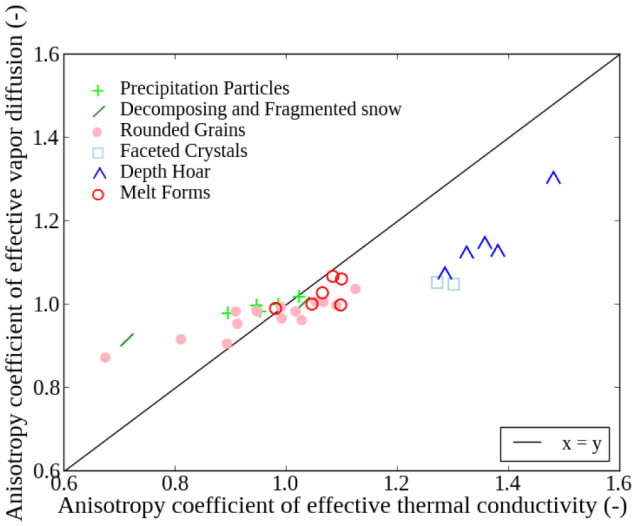

Figure 10. Anisotropy coefficients of effective vapor diffusion versus the anisotropy coefficients of effective thermal conductivity. The latter come from Calonne et al.[37] Colors and symbols correspond to the ICSSG.[37]

diffusion versus the anisotropy coefficient of the effective thermal conductivity. The latter comes from the study of Calonne et al.[37] The anisotropy coefficient of the effective vapor diffusion ranges from 0.86 for a natural snow sample of rounded grains collected in depth to 1.29 for a particularly evolved depth hoar sample obtained in cold room. In contrast with the coefficient of the effective thermal conductivity, the anisotropy coefficient of the effective vapor diffusion does not separate systematically the depth hoar and faceted crystals from the other snow types. Overall, the effective vapor diffusion shows a more isotropic behavior (values centered around 1) than the effective thermal conductivity.

Finally, in Figure 9 we have also reported (i) the cold-room measurements of the effective vapor diffusion in snow performed by Sokratov and Maeno[24] and (ii) the self-consistent estimate of the effective diffusion for spherical inclusions:[29] $D^{SC} = D_v(3\phi - 1)/2$. The experimental values of Sokratov and Maeno,[24] which are smaller than 1 and tend to indicate that there is no enhancement of the effective vapor diffusion in snow, are in overall much higher than our numerical values. The self-consistent formula offers a good estimate of our numerical results, within an averaged relative error of ±10%.

DISCUSSION

In the presented paper, the macroscopic equivalent modeling of heat and water vapor transfer through snow has been derived from the physics at the pore scale by using an upscaling method. In the absence of convection and densification, we have shown that this macroscopic equivalent modeling strongly depends on the order of magnitude of dimensionless numbers defined at the ice−pore interface ([H] and [W]). In the most general case (Case 1: $[H] = O(\varepsilon^2)$ and $[W] = O(\varepsilon^2)$), the heat and mass transfer are described by two coupled equations including a source term $Q_T = SSA_V L_{sg} w_n^{(0)}$ and $Q_V = -SSA_V \rho_i w_n^{(0)}$, where $w_n^{(0)}$ is given by the Clausius−Clapeyron's law and the Hertz−Knudsen equation expressed in terms of macroscopic variables. The obtained macroscopic modeling is similar to the one presented by Albert and McGilvary[11] in a phenomenological way. By contrast, the homogenization process also provides the definition of the effectives properties and of the domain of validity of the modeling via the dimensionless numbers.

The macroscopic description was derived for a condition of scale $\varepsilon = 5 \times 10^{-3}$. This corresponds to a "medium" separation of scale and higher values will indicate that microscopic and macroscopic scales cannot be separated; the homogenization method will thus not be applicable. Inversely, as shown by eq 19, the smaller the condition of the scale, the closer the macroscopic description with respect to the microscopic one. In that case, the source terms at the interface will have less influence on the macroscopic profile of vapor and heat.

On the basis of the definition of Q_v and Q_T, the mass transfer coefficient at the interface h_m, which is expressed in the source terms presented by Albert and McGilvary,[11] is perfectly defined as

$$h_m = \frac{\rho_i}{\beta \rho_{vs}^{(0)}(T^{(0)})} \tag{35}$$

Figure 11 shows the mass transfer coefficient as a function of the temperature and for three values of β. The gray zone

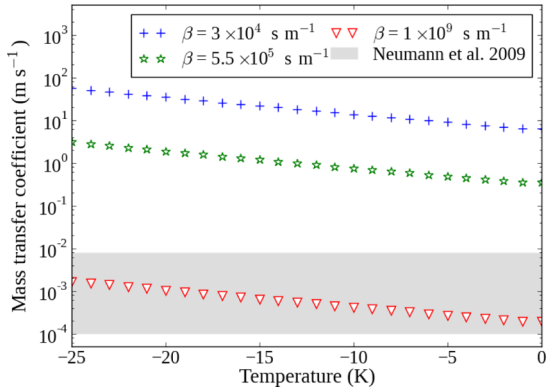

Figure 11. Mass transfer coefficient as a function of temperature, computed with eq 35 using three values of the interface kinetic coefficient β. Values of $\rho_{vs}^{(0)}$ are computed using the Clausius−Clapeyron law (see eq 23) and ρ_i is equal to 917 kg m^{-3}. The range of values corresponding to the measurements of Neumann et al.[12] are shown by the gray area.

corresponds to the range of values of h_m measured by Neumann et al.[12] The mass transfer coefficient decreases with increasing temperature and its order of magnitude strongly depends on β. To be in agreement with the experimental data of Neumann et al.,[12] the mass transfer must be computed with a value of β around 1×10^9 s m^{-1}.

In all modeling cases, the effect of phase changes occurring at the micro scale is larger on the macroscopic vapor field than in the macroscopic temperature field, as suggested in Figure 2. Indeed, the relative errors observed for the temperature profiles of Figure 5 remain small with and without taking into account Q_T in the macroscopic modelings. This observation is consistent with the parametric study performed by Albert and McGilvary.[11] Nevertheless, the above considerations are counterbalanced by the fact that, because the evolution of the saturation vapor density over ice is exponential with respect to the temperature, a small error in the macroscopic temperature induces a large error in the macroscopic vapor density. This error is enhanced for the large temperature gradients. In conclusion, the effect of phases changes at the macro scale

dx.doi.org/10.1021/jp5052535 | J. Phys. Chem. B 2014, 118, 13393−13403

should be taken into account via Q_T and Q_v for a better precision, and especially when snow experiences large temperature gradients.

In agreement with Sokratov and Maeno[24] and Pinzer et al.,[19] our theoretical developments and 3D image-based computations of the effective vapor diffusion tensor $\mathbf{D}^{\mathrm{eff}}$ indicate that there is no enhancement of the effective vapor diffusion in snow. In the absence of convection, the sublimation and deposition over the ice surface, which can be viewed as a mechanism that enhances the vapor transfer, is reflected by the macroscopic source term Q_v and not by $\mathbf{D}^{\mathrm{eff}}$. The good agreement of the vapor density profiles of the 2D snow layer between the microscopic and macroscopic modeling strengthens the above considerations. Our results of effective vapor diffusion are overall smaller than the values of Sokratov and Maeno,[24] who first present a non-enhanced effective vapor diffusion based on experimental results. The scatter of the data of Sokratov and Maeno[24] highlights the difficulty of performing such measurements.

Further developments are required concerning the following points: (i) Case 0, i.e., when $[\mathrm{H}] = O(\varepsilon^2)$ and $[\mathrm{W}] = O(\varepsilon)$ has not been investigated in the present work. This case corresponds typically to snow layers under very large temperature gradients. These gradients may lead to a macroscopic length associated with the phenomena (ratio between the average temperature over the temperature gradient) smaller than the geometric one associated with the thickness of the snow layer, and consequently to a poor separation of scales.[40] In that case, the macroscopic modeling can be formulated by investigating the following superior order of approximation in the asymptotic analysis. (ii) A poor separation of scales can also occur when the thickness of the snow layer L is very small. Such a particular case can be studied as in the Case 0, by investigating the following superior order of approximation in the asymptotic analysis. (iii) In the present modeling, the air convection, which can be induced by wind-pumping,[41] for example, has been neglected. These effects must be included in the microscopic description to quantify their influences (convection, dispersion, etc.) on the macroscopic modeling. (iv) Monitored experiments might be carried out to evaluate the macroscopic modeling with respect to measurements.

CONCLUSION

In this paper, we derived the macroscopic equivalent modeling of the heat and water vapor transfer through snow from its description at the pore scale using the homogenization of multiple scale expansions.[25−27,29] In contrast with more phenomenological models, the homogenization method provides the exact expression of the effective properties and the source terms (i.e., the mass transfer coefficient) at the macroscopic scale. The formulation of the macroscopic equivalent modeling is driven by the order of magnitude of the dimensionless numbers that characterize the physics at the pore scale, and thus constitute the domain of validity of the modeling.

In the most general case, the macroscopic modeling is described by two coupled equations of heat and vapor transfer including a source term. These source terms arise from the phase changes at the ice−air interface. The upscaling process clearly shows that these phase changes do not appear in the definition of the effective properties (effective diffusion, effective thermal conductivity, etc.), in contradiction with some macroscopic models presented in the literature.[42,43]

The precision and the robustness of the obtained macroscopic equivalent modeling were evaluated by comparing the results of numerical simulations of the heat and the water vapor transfer through a snow layer obtained in the case of a fine scale modeling (i.e., taking into account all the heterogeneities) and in the case of the corresponding macroscopic modeling, for temperature gradients ranging from 50 to 250 K m^{-1}. This study points out that (i) the temperature field is estimated by the obtained macroscopic modeling within a smaller error than the water vapor density field (both errors increase with increasing temperature gradients) and (ii) the macroscopic source term of heat and vapor is required in the macroscopic modeling especially for snow which experiences large temperature gradients.

Finally, the effective diffusion tensor involved in the macroscopic modeling has been computed using the result of the homogenization method on 3D images of different snow types. The effective diffusion coefficients of snow are lower than the one of air, decrease gradually with increasing density, and exhibit a slight anisotropy for some snow samples. The self-consistent formula provides a good estimation of our coefficients with respect to the snow density. Our theoretical developments and numerical results indicate that the vapor diffusion is not enhanced in snow.

ASSOCIATED CONTENT

Supporting Information

Detailed equations of the homogenization process (Appendix A) and normalized values of the x, y, and z components of the effective vapor diffusion tensor (Appendix B). This material is available free of charge via the Internet at http://pubs.acs.org/.

AUTHOR INFORMATION

Corresponding Authors

*N. Calonne. E-mail: neige.calonne@meteo.fr.

*C. Geindreau. E-mail: christian.geindreau@3sr-grenoble.fr.

Notes

The authors declare no competing financial interest.

ACKNOWLEDGMENTS

Funding by Météo-France and DigitalSnow (ANR-11-BS02-009) is acknowledged. We thank Samuel Morin, Pierre Spandre, and two anonymous reviewers for useful suggestions that improved the quality of the manuscript. The tomographic images were obtained at the ESRF (ID19) and 3SR-Lab. CNRM-GAME/CEN is part of the Labex OSUG@2020 (ANR10 LABX56). 3SR lab is part of the LabEx Tec 21 (Investissements d'Avenir - grant agreement ANR-11-LABX-0030).

REFERENCES

(1) Schweizer, J.; Jamieson, B.; Schneebeli, M. Snow avalanche formation. *Rev. Geophys.* **2003**, *41*.

(2) Grannas, A. M.; Jones, A. E.; Dibb, J.; et al. An overview of snow photochemistry: evidence, mechanisms and impacts. *Atmos. Chem. Phys.* **2007**, *7*, 4329−4373.

(3) Sokratov, S. A.; Barry, R. G. Intraseasonal variation in the thermoinsulation effect of snow cover on soil temperatures and energy balance. *J. Geophys. Res.: Atmos. (1984−2012)* **2002**, *107*, ACL−13.

(4) Christon, M.; Burns, P. J.; Sommerfeld, R. A. Quasi-steady temperature gradient metamorphism in idealized, dry snow. *Numer. Heat Transfer, Part A* **1994**, *25*, 259−278.
(5) Flin, F.; Brzoska, J.-B.; Lesaffre, B.; Coléou, C.; Pieritz, R. A. Full three-dimensional modelling of curvature-dependent snow metamorphism: first results and comparison with experimental tomographic data. *J. Phys. D: Appl. Phys.* **2003**, *36*, A49−A54.
(6) Kaempfer, T.; Schneebeli, M.; Sokratov, S. A microstructural approach to model heat transfer in snow. *Geophys. Res. Lett.* **2005**, *32*, L21503.
(7) Brzoska, J.-B.; Flin, F.; Barckicke, J. Explicit iterative computation of diffusive vapour field in the 3-D snow matrix: preliminary results for low flux metamorphism. *Ann. Glaciol.* **2008**, *48*, 13−18.
(8) Flin, F.; Brzoska, J.-B. The temperature gradient metamorphism of snow: vapour diffusion model and application to tomographic images. *Ann. Glaciol.* **2008**, *49*, 17−21.
(9) Kaempfer, T. U.; Plapp, M. Phase-field modeling of dry snow metamorphism. *Phys. Rev. E* **2009**, *79*, 031502.
(10) Vetter, R.; Sigg, S.; Singer, H.; Kadau, D.; Herrmann, H.; Schneebeli, M. Simulating isothermal aging of snow. *Europhys. Lett.* **2010**, *89*, 26001.
(11) Albert, M.; McGilvary, W. Thermal effects due to air flow and vapor transport in dry snow. *J. Glaciol* **1992**, *38*, 273−281.
(12) Neumann, T. A.; Albert, M. R.; Engel, C.; Courville, Z.; Perron, F. Sublimation rate and the mass-transfer coefficient for snow sublimation. *Int. J. Heat Mass Transfer* **2009**, *52*, 309−315.
(13) Jordan, R. E. *A one-dimensional temperature model for a snow cover*. Technical documentation for SNTHERM.89; U.S. Army Corps of Engineers, Cold Regions Research and Engineering Laboratory: Hanover, NH, 1991.
(14) Brun, E.; David, P.; Sudul, M.; Brunot, G. A numerical model to simulate snow-cover stratigraphy for operational avalanche forecasting. *J. Glaciol.* **1992**, *38*, 13−22.
(15) Lehning, M.; Bartelt, P.; Brown, B.; Russi, T.; Stöckli, U.; Zimmerli, M. SNOWPACK model calculations for avalanche warning based upon a new network of weather and snow stations. *Cold Reg. Sci. Technol.* **1999**, *30*, 145−157.
(16) Vionnet, V.; Brun, E.; Morin, S.; Boone, A.; Martin, E.; Faroux, S.; Moigne, P. L.; Willemet, J.-M. The detailed snowpack scheme Crocus and its implementation in SURFEX v7.2. *Geosci. Model. Dev.* **2012**, *5*, 773−791.
(17) Yen, Y.-C. *Review of the thermal properties of snow, ice and sea ice*; U.S. Army Corps of Engineers, Cold Regions Research and Engineering Laboratory: Hanover, NH, 1981.
(18) Lehning, M.; Bartelt, P.; Brown, B.; Fierz, C.; Satyawali, P. A physical SNOWPACK model for the Swiss avalanche warning. Part II: snow microstructure. *Cold Reg. Sci. Technol.* **2002**, *35*, 147−167.
(19) Pinzer, B.; Schneebeli, M.; Kaempfer, T. Vapor flux and recrystallization during dry snow metamorphism under a steady temperature gradient as observed by time-lapse micro-tomography. *Cryosphere* **2012**, *6*, 1141−1155.
(20) Yosida, Z.; Oura, H.; Kuroiwa, D.; Huzioka, T.; Kojima, K.; Aoki, S.; Kinosita, S. Physical Studies on Deposited Snow. I. Thermal Properties. *Contrib. Inst. Low Temp. Sci., Hokkaido Univ.* **1955**, *7*, 19−74.
(21) Colbeck, S. The vapor diffusion coefficient for snow. *Water Resour. Res.* **1993**, *29*, 109−115.
(22) Sturm, M.; Holmgren, J.; König, M.; Morris, K. The thermal conductivity of seasonal snow. *J. Glaciol.* **1997**, *43*, 26−41.
(23) Satyawali, P. Diffusivity and vapor flow into snow during phase change. *Ann. Glaciol.* **2000**, *31*, 445−450.
(24) Sokratov, S. A.; Maeno, N. Effective water vapor diffusion coefficient of snow under a temperature gradient. *Water Resour. Res.* **2000**, *36*, 1269−1276.
(25) Bensoussan, A.; Lions, J.-L.; Papanicolaou, G. *Asymptotic Analysis for periodic structures*; North Holland: Amsterdam, 1978.
(26) Sanchez-Palencia, E. *Non-homogeneous media and vibration theory*; Lectures Notes in Physics, Vol. *127*; Springer-Verlag: Berlin, 1980.
(27) Auriault, J.-L. Heterogeneous medium. Is an equivalent description possible? *Int. J. Eng. Sci.* **1991**, *29*, 785−795.
(28) Geindreau, C.; Auriault, J.-L. Transport Phenomena in Saturated Porous Media under Liquid-Solid Phase Change. *Arch. Mech.* **2001**, *53*, 385−420.
(29) Auriault, J.-L.; Boutin, C.; Geindreau., C. *Homogenization of coupled phenomena in heterogenous media*; Wiley-ISTE: London, 2009.
(30) Auriault, J. Heterogeneous periodic and random media. Are the equivalent macroscopic descriptions similar? *Int. J. Eng. Sci.* **2011**, *49*, 806−808.
(31) Barrett, J. W.; Garcke, H.; Nürnberg, R. Numerical computations of faceted pattern formation in snow crystal growth. *Phys. Rev. E* **2012**, *86*, 011604.
(32) Libbrecht, K. G. The physics of snow crystals. *Rep. Prog. Phys.* **2005**, *68*, 855−895.
(33) Massman, W. A review of the molecular diffusivities of H_2O, CO_2, CH_4, CO, O_3, SO_2, NH_3, N_2O, NO, and NO_2 in air, O_2 and N_2 near STP. *Atmos. Environ.* **1998**, *32*, 1111−1127.
(34) Colbeck, S. C. Theory of metamorphism of dry snow. *J. Geophys. Res.* **1983**, *88*, 5475−5482.
(35) Fukuzawa, T.; Akitaya, E. Depth-hoar crystal growth in the surface layer under high temperature gradient. *Ann. Glaciol.* **1993**, *18*, 39−45.
(36) Libbrecht, K.; Rickerby, M. Measurements of growth rates of (0001) ice crystal surfaces. arXiv:1110.5828 [cond-mat.mtrl-sci], 2011.
(37) Calonne, N.; Flin, F.; Morin, S.; Lesaffre, B.; Rolland du Roscoat, S.; Geindreau, C. Numerical and experimental investigations of the effective thermal conductivity of snow. *Geophys. Res. Lett.* **2011**, *38*, L23501.
(38) Calonne, N.; Geindreau, C.; Flin, F.; Morin, S.; Lesaffre, B.; Rolland du Roscoat, S.; Charrier, P. 3-D image-based numerical computations of snow permeability: links to specific surface area, density, and microstructural anisotropy. *Cryosphere* **2012**, *6*, 939−951.
(39) Fierz, C.; Armstrong, R. L.; Durand, Y.; Etchevers, P.; Greene, E.; McClung, D. M.; Nishimura, K.; Satyawali, P. K.; Sokratov, S. A. *The international classification for seasonal snow on the ground*; IHP-VII Technical Documents in Hydrology no. 83; IACS Contribution no. 1; UNESCO: Paris, 2009.
(40) Auriault, J.-L.; Geindreau, C.; Boutin, C. Filtration law in porous media with poor separation of scales. *Transp. Porous Media* **2005**, *60*, 89−108.
(41) Albert, M. R.; Shultz, E. F. Snow and firn properties and air-snow transport processes at Summit, Greenland. *Atmos. Environ.* **2002**, *36*, 2789−2797.
(42) Sun, S.; Jin, J.; Xue, Y. A simple snow-atmosphere-soil transfer model. *J. Geophys. Res.: Atmos. (1984−2012)* **1999**, *104*, 19587−19597.
(43) Boone, A.; Etchevers, P. An intercomparison of three snow schemes of varying complexity coupled to the same land-surface model: Local scale evaluation at an Alpine site. *J. Hydrometeorol.* **2001**, *2*, 374−394.

NOTE ADDED AFTER ASAP PUBLICATION

This paper published ASAP on July 28, 2014. Corrections were made to the Results section and in the caption for Figure 4. The revised version was reposted on July 29, 2014.